6.1. Introduction

In the past few years, the science and technology of nanomaterial have been rapidly advancing to develop the materials which have high dielectric permittivity. The nanocomposite materials depend not only on the properties of their individual component but also on their bulk morphology and interfacial characteristics. The nanocomposite finds their use in various applications because of the improvements in the properties over the simpler structures. Hence these materials are promising for technological applications such as miniaturization of electronic devices for microelectronics, capacitors, and energy storage systems. They have high breakdown field strength of metal oxides with high permittivity of ABO_3 type oxides [Moulson & Herbert *et al*. (2003)]. The composite materials exhibiting a high dielectric constant are either perovskite-based ferroelectric ceramics such as undoped or doped $BaTiO_3$ or the relaxor ferroelectrics including $Pb(Mg_{1/3}Nb_{2/3})O_3$[PMN], $Pb(Zn_{1/3}Nb_{2/3})O_3$[PZN] and $Pb_{1-x}La_x(Zr_{1-y}Ti_y)O_3$[PLZT] [Yadava *et al*. (2016)]. The dielectric constant is highly unstable depending on temperature, and it is not suitable for a high-temperature application. High-temperature ferroelectric materials exhibiting a phase transition near the Curie temperature are also not ideal choices for applications [Gautam *et al*. (2017)]. $Bi_{2/3}Cu_3Ti_4O_{12}$ is one of the members of $ACu_3Ti_4O_{12}$ type materials which is isostructurally similar to $CaCu_3Ti_4O_{12}$ (CCTO). CCTO has high dielectric constant ($\varepsilon' \sim 10^4$) and excellent thermal stability in the wide temperature range from 100 - 600 K [Subramanian *et al*. (2000)]. It is broadly utilized in the production of electronic components such as DRAM (Dynamic Random Access Memory), microwave devices, electronic devices and multilayer capacitors in automobiles and aircraft [Singh *et al*. (2011), Cheng *et al*. (2004), Home *et al*. (2001), Li *et al*. (2010), Kwon *et al*. (2008)]. Consequently, the task is to develop a material with high energy density without a substantial rise in dielectric loss, and also with higher dielectric field strength and dielectric permittivity. Recently, we have reported the

dielectric properties of $0.5Bi_{2/3}Cu_3Ti_4O_{12}$-$0.5BaTiO_3$ composite, and its dielectric constant and dielectric loss were found to be ≈ 506 and ≈ 2.70, respectively at room temperature (303 K) and 1 kHz [Khare *et al*. (2017)]. The dielectric constant of this composite is very high, but its dielectric loss is also high. So we have slightly changed the composition of the composite to see the effect of dielectric properties. The synthesis of nanoscale materials has presented many challenges regarding the control of size and shape by adopting various synthesis procedures [Jie *et al*. (2004), Zhang *et al*. (2011), Patrinoiu *et al*. (2012)].

In this work, $0.6Bi_{2/3}Cu_3Ti_4O_{12}$-$0.4BaTiO_3$ (BC-BT) nanocomposite has been synthesized using the modified solid state route. The dielectric and AC impedance spectroscopic analysis were carried out of the BC-BT composite. Studying the dielectric data on different functions allows various features of the composite on the dielectric anomalies in the composite ceramic. The study of impedance is presented here to reveal the effect of the grain, grain boundary interaction and the electrode interfaces on the conduction mechanism. To the best of our knowledge, the consequences presented here are not reported earlier. The nanocomposite ceramic has been characterized by different physicochemical techniques and its dielectric, and electrical behavior is reported here.

6.2. Experimental

6.2.1. Synthesis of materials

The nanocomposite ceramic, $0.6Bi_{2/3}Cu_3Ti_4O_{12}$-$0.4BaTiO_3$, was synthesized by a modified solid-state method in three steps using calcined powders of $Bi_{2/3}Cu_3Ti_4O_{12}$ and $BaTiO_3$ prepared by citric and assisted combustion synthesis. First, $Bi_{2/3}Cu_3Ti_4O_{12}$ was synthesized by a semi-wet route using $Bi(NO_3)_2.4H_2O$ (99.5% Qualigens, India), $Cu(NO_3)_2.3H_2O$ (99.5% Merck, India), solid TiO_2 (99.5% Merck, India), as starting materials.

Solid TiO_2 was mixed with nitrate solutions of metal ions. Second, $BaTiO_3$ ceramic powder was synthesized by the semi-wet route using $Ba(NO_3)_2$, TiO_2 (99.5% Merck, India), and citric acid (99.5% Merck, India) as starting materials. The metal nitrates were dissolved in doubly distilled water to obtain standard aqueous solutions of Bi^{3+}, $Ba^{2+}$and Cu^{2+} ions. Stoichiometric amounts of the stock aqueous solutions of Bi^{3+} and Cu^{2+} used in the synthesis of $Bi_{2/3}Cu_3Ti_4O_{12}$ and Ba^{2+} solution for $BaTiO_3$ were mixed in separate beakers along with stoichiometric quantities of solid TiO_2. Then, citric acid was added to the solutions. The resulting dispersion was heated at 70 – 80 °C on a hot plate magnetic stirring to evaporate water which finally gives a lot of gases and produced a fluffy mass of $Bi_{2/3}Cu_3Ti_4O_{12}$ and $BaTO_3$ ceramic powders on combustion.

The technique involves the mixing of solutions of a metal precursor and an organic polyfunctional acid possessing at least one carboxylic acid group and one hydroxyl group such as citric, glycine, tartaric or glycerol which results in complexation of the metal by poly-carboxylic acid. Citric acid acts as complexing agents which form a complex with cations at both the carboxylic end and afford the fuel for the ignition step. The regulator increases the temperature to form a very fine crystalline precursor powder [Singh *et al*. (2013)]. The foamy products of $Bi_{2/3}Cu_3Ti_4O_{12}$ and $BaTO_3$ were collected and calcined in air at 800 °C for 8 h in an electric furnace. Thirdly, an appropriate amount of the prepared powders of $Bi_{2/3}Cu_3Ti_4O_{12}$ and $BaTO_3$ by a citric acid assisted sol–gel process was mixed and reground in acetone using an agate mortar for 24 h to form a composite.

In this method, we used the $Bi_{2/3}Cu_3Ti_4O_{12}$ and $BaTiO_3$ (0.60:0.40 M proportion) calcined powder as raw materials to synthesize the BC-BT nanocomposite ceramic. We developed the new modified solid state route to get nanometer crystalline powder with the desired properties. The powder was mixed with polyvinyl alcohol (PVA 2 wt. %) and pressed into cylindrical pellets using a hydraulic press. The PVA binder was burnt out at 350

°C for 2 h. Finally, the BC-BT pellets were sintered at 870 °C for 4 h, 8 h, 12 h, and 16 h in air.

6.2.2. Structural and microstructural characterization

The phase composition of the samples was revealed by using the X-ray diffraction analysis (Rigaku, miniflex-600, Japan) employing Cu-Kα radiation. The BC-BT composite was scanned at 0.02 °/min over the 2θ range of 20–80°. Images of the microstructure were studied using a scanning electron microscope (SEM, ZEISS, model EVO18, Germany) and the particle size was evaluated using a high-resolution transmission electron microscope (TEM, Tecnai G^2 20 TWIN). The specimen for TEM analysis was prepared by dispersing the sintered BC-BT powder in acetone by ultra-sonication. A drop of suspension was added to the carbon-coated copper grid and dried in a hot air oven. The surface morphology was analyzed by atomic force microscopy [AFM NTEGRA Prima, Germany]. The specimens were prepared by dispersing the sintered BC-BT nanocomposite powders in acetone by ultra-sonication, and this type of suspensions was deposited onto the glass slides. The magnetic measurement was carried out with a quantum design MPMS-3, over a temperature range 5-100 K and applied a magnetic field of 2 T. Temperature-dependent Zero field cooling (ZFC) and field cooling (FC) magnetization was also recorded at 100 Oe applied field using SQUID VSM dc magnetometer in the same temperature range.

6.2.3. Dielectric and electrical measurements

Dielectric and electric measurements were made using a pellet which both surfaces were polished and coated with silver paint which was then dried at 200 °C for 15 min and cooled naturally to room temperature. The dielectric and electrical data of the BC-BT

ceramics was collected using an impedance analyzer (PSM 1735, NumetriQ 4th Ltd, and U.K) over a frequency range of 10^2–10^6 Hz, and in the temperature range of 300–500 K.

6.3. Results and Discussion

6.3.1. X-ray diffraction studies

Figure. 6.1 shows XRD pattern of the BC-BT ceramic composite sintered at 870 °C for 4 h, 8 h, 12 h and 16 h. The XRD pattern of the ceramic illustrates the presence of minor phases $BaTO_3$ and major phase $Bi_{2/3}Cu_3Ti_4O_{12}$. The main peaks of the ceramic substantiate the results to those of the standard ceramic XRD pattern of $Bi_{2/3}Cu_3Ti_4O_{12}$ (JCPDS – 80-1343) and $BaTO_3$ (JCPDS – 89-2475) which confirmed the formation of the composite sintered at 870 °C. XRD also shows the presence of split peaks for reflections (220), (110) and (200) due to the presence of Cu-$K\alpha_2$ along with Cu-$K\alpha_1$ in the X-ray radiation used for diffraction. The intensities of peaks from Cu-$K\alpha_2$ are close to 50% of the intensity of the corresponding peak from Cu-$K\alpha_1$ which is supported by the above fact as expected [Singh *et al*. (2014), Yang *et al*. (2015)].

X-Ray diffraction data is also used to determine the mean crystallite size (D) of the BC-BT composite ceramic using line broadening method. In the single-line analysis process, the Cauchy component of the Voigt function reveals crystallite size given by the equation 2.2. The average crystallite sizes derived from the XRD data were found to be 35 nm, 26 nm, 17 nm and 22 nm for the BC-BT ceramic sintered for 4 h, 8 h, 12 h and 16 h, respectively.

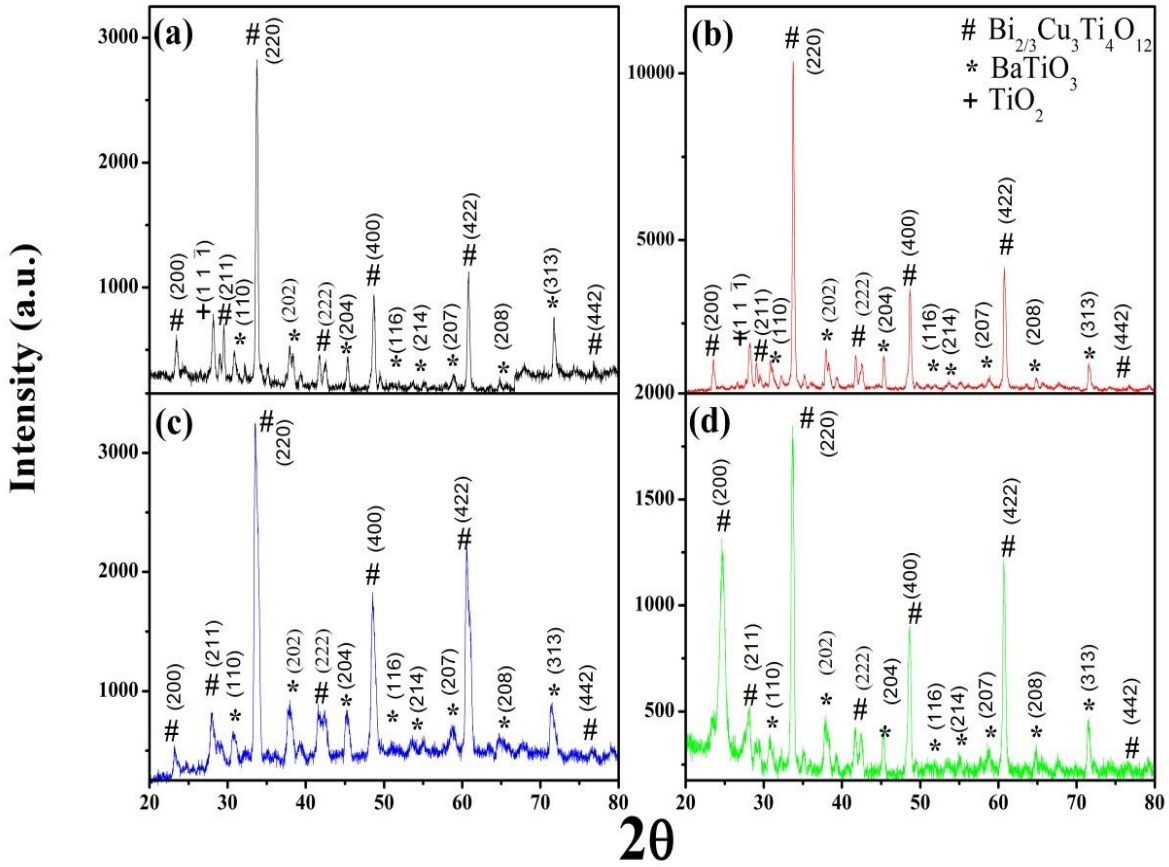

Figure 6.1. X-ray powder diffraction pattern of a BC-BT nanocomposite sintered at 870 °C for **(a)** 4 h **(b)** 8 h **(c)** 12 h and **(d)** 16 h.

6.3.2. Microstructural studies

Figure 6.2(a) shows the bright field TEM image of the BC-BT nanocomposite ceramic sintered at 870 °C for 12 h. The particle size of the BC-BT ceramic composite was 70 ± 10 nm, suggesting that the ceramic powder was nanocrystalline in nature. The particles sizes observed by TEM are larger than the average crystallite size determined by XRD. These differences could be attributed due to the formation of particles with the combination of few crystallites.

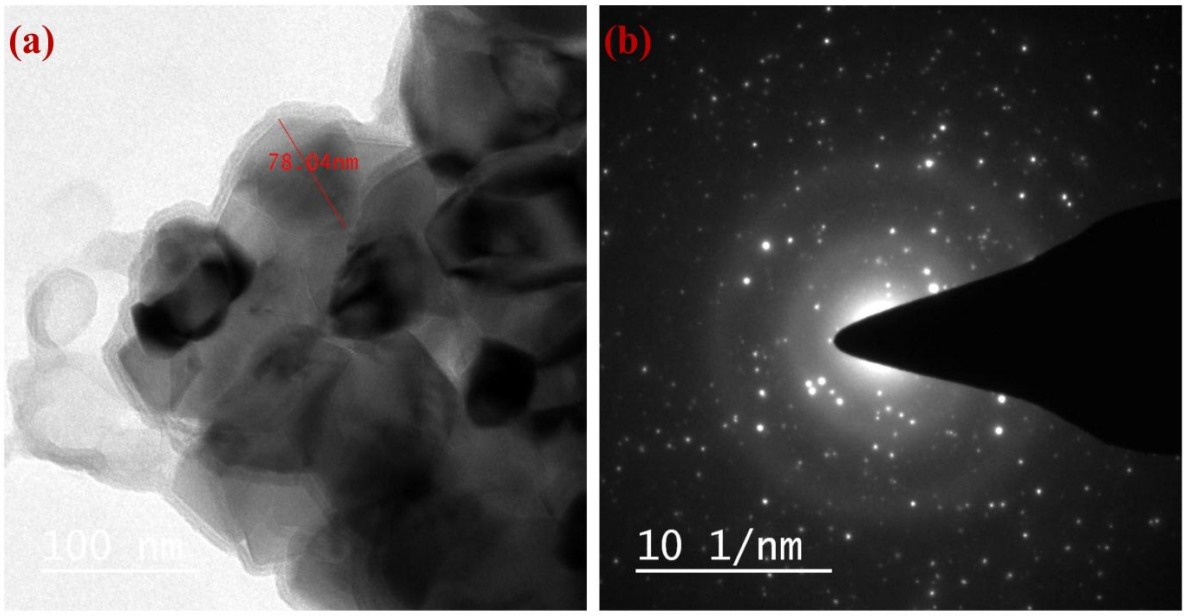

Figure 6.2 (a) Bright field TEM images and **(b)** SEAD pattern of a BC-BT nanocomposite sintered at 870 °C for 12 h.

Figure 6.2(b) shows the selected area electron diffraction patterns (SAED) of the BC-BT composite ceramic which confirmed the presence of nanocrystalline nature. The interplanar spacings (d_{hkl}) measured from the SAED are in good agreement with the values obtained from XRD pattern of $Bi_{2/3}Cu_3Ti_4O_{12}$ ((JCPDS – 80-1343) and $BaTO_3$ (JCPDS – 89-2475).The additional spots were also observed in the SAED patterns implying the contribution from adjacent grains and subgrains arising due to their orientation difference in different directions.

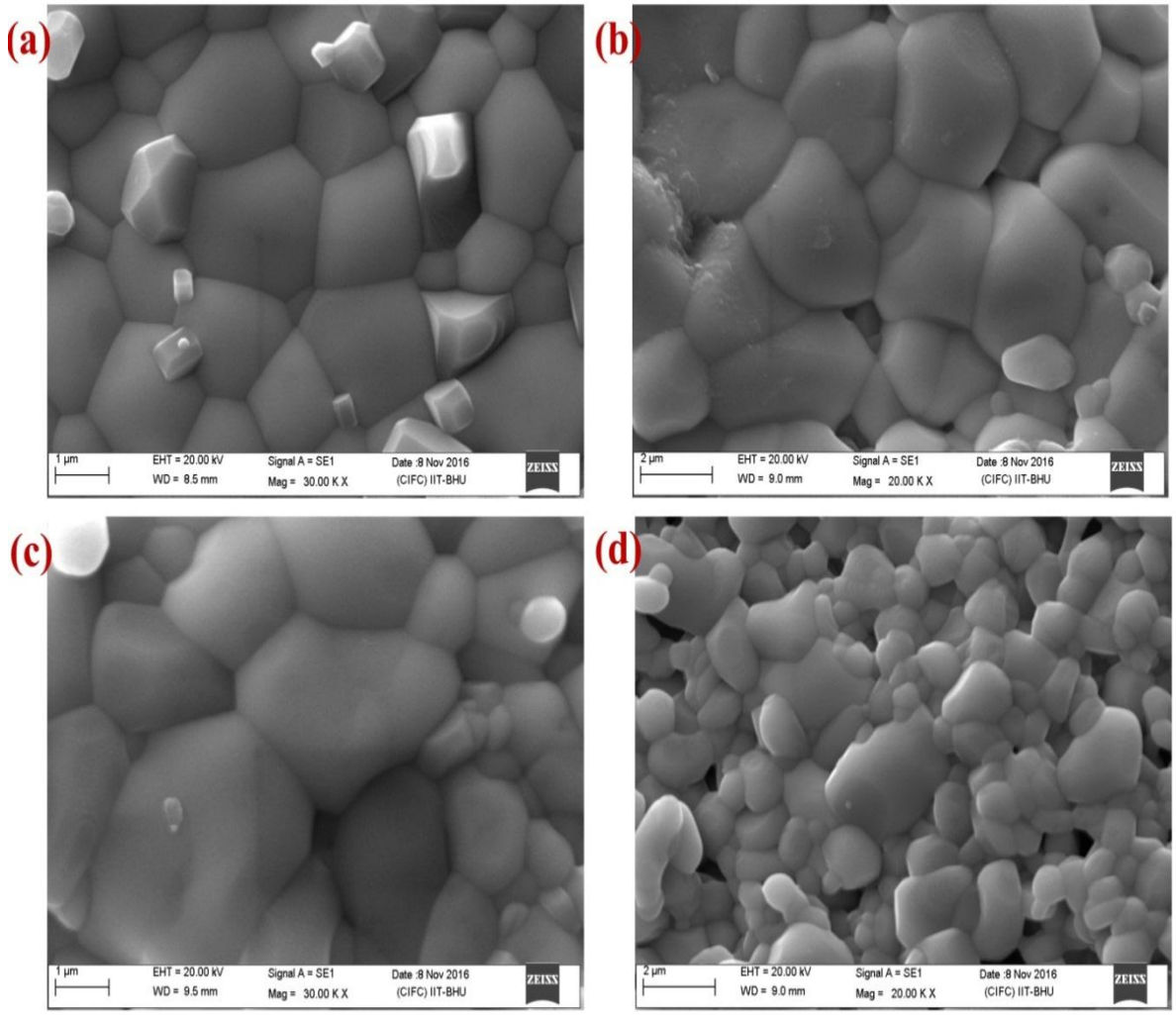

Figure 6.3. SEM image of a BC-BT nanocomposite sintered at 870 °C for **(a)** 4 h **(b)** 8 h **(c)** 12 h and **(d)** 16 h.

The microstructure of fractured surface of the BC-BT ceramic sintered at 870 °C for 4 h, 8 h, 12 h and 16 h is shown in Figure 6.3. The average grain size of the BC-BT nanocomposite observed from SEM estimated was found to be 2.03 µm, 2.92 µm, 2.11 µm and 2.38 µm sintered at 870 °C for 4 h, 8 h, 12 h and 16 h, respectively. SEM image for BC-

BT ceramic revealed the presence of abnormally large grains having a size in the range 2–3 μm. It has a few duplex microstructure consisting of very few large grains over 3 μm size isolated by regions composed of fine grains of 0.50–1.0 μm, and thus it supports the bimodal nature of CCTO reported earlier [Shao *et al*. (2006), Krohns *et al*. (2007)]. Further, the particles of BC-BT ceramic have smooth surfaces associated with a spherical appearance, and similar microstructure published recently in BTO-CCTO composite [Kim *et al*. (2013)].

Figure 6.4(a) clearly shows that grains and grain boundaries of 2D AFM image of the BC-BT nanocomposite ceramic sintered at 870 °C for 12 h. Although, the height and roughness of the BC-BT sample is decreased with the increase in the sintering duration as observed in 3D AFM images [Karnik *et al*. (2006)]. The average thickness characterized surface morphologies, and the roughness parameters such as average roughness (R_a), Root mean square roughness (RMS) of the BC-BT specimen. The parameter R_a is the average value for the surface about the central plane. RMS is the mean difference in height among the four highest peaks and the four lowest valleys, and R_{max} is the maximum peak about the central plane in the analyzed area as shown in Figure 4(c). The average roughness and root mean square (RMS) data were obtained as 4.64 nm and 6.75 nm respectively on scanned area 10 μm × 10 μm where ten different points were used for the calculation of mean value [Khulbe *et al*. (1996), Khare *et al*. (2016), Yadava *et al*. (2016)]. The average grain size estimated from two-dimensional images was found to be 0.41 μm after taking into account of 118 grains as shown in the histogram Figure 6.4(d).

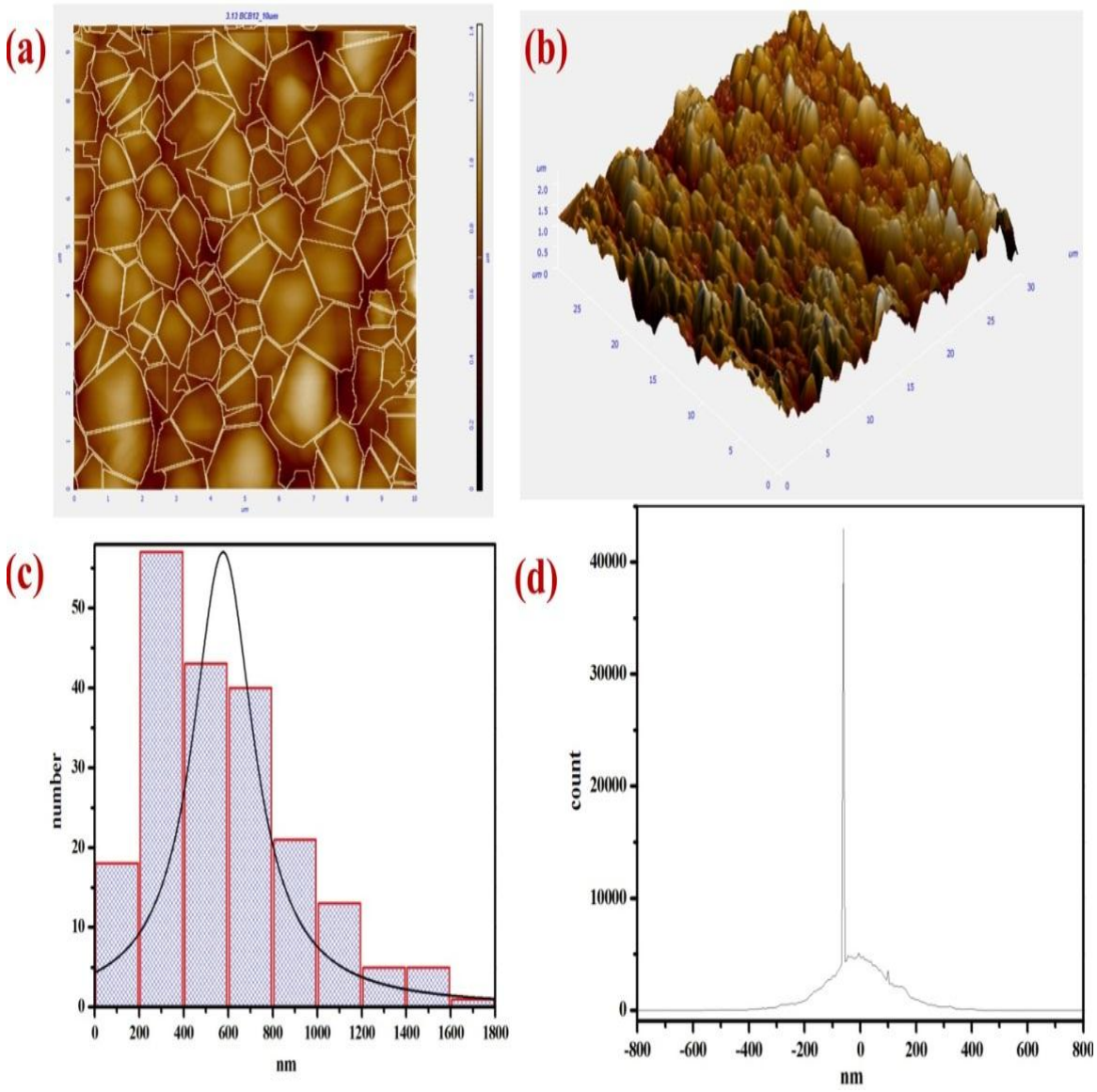

Figure 6.4. AFM images of BC-BT nanocomposite sintered at 870 °C for 12 h **(a)** 2 dimensional **(b)** 3D Structure **(c)** bar diagram of particles size **(d)** depth histogram.

6.3.3. Magnetic measurements

Figure 6.5 shows the magnetization curve of zero fields cooled (M^{ZFC}) and field cooled (M^{FC}) at the temperature of 5-100 K with applied field 100 Oe. Figure 5 (a) shows the ZFC and FC curve merge to each other. Below the 27 K, both curves increase parallel with increasing temperature and decreasing magnetization. ZFC and FC curve shows a broad peak at 27 K with increasing magnetization. The behavior of composite materials shows phase transition from ferromagnetic to paramagnetic. This temperature is known as Curie temperature [Gautam *et al*. (2016)].

Figure 6.5(b). Shows the M-H hysteresis loops of BC-BT composite ceramic as a magnetization function of the magnetic field measured ± 2T at 5K, 50K, and 100K. It is revealed from a figure that the remnant magnetization (M_r) and coercivity (H_c) of material acquired increase with the increase of temperature. However, the extension of hysteresis loop observed in the low magnetic field was shown in the insect, which confirms the paramagnetic behavior and exhibits weak ferromagnetic moment.

The magnetic parameter of BC-BT composite ceramic was given in table. 6.1. The lower coercivity value of BC-BT composite ceramics shows soft magnetic materials.

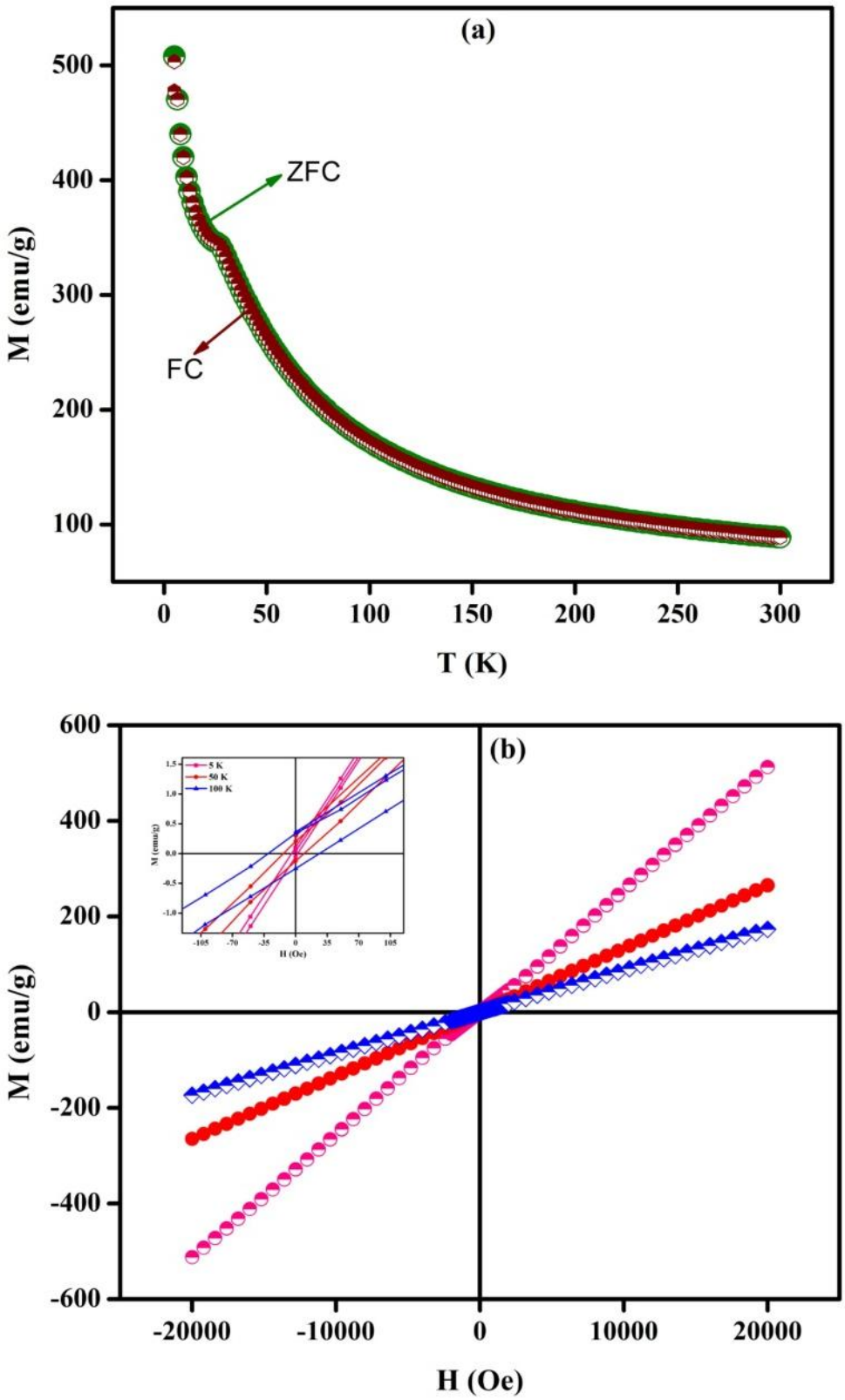

Figure 6.5. (a) Temperature-dependent zero field cooled (ZFC) and field cooled (FC) magnetization measured at H=100 Oe, **(b)** magnetization (M) versus applied field (H) for the BC-BT composite ceramic.

Table 6.1 The magnetic parameters of BCB nanocomposite ceramic

Temperature (K)	M_r (emu/g)	H_c (Oe)
5 K	0.1043	3.2656
50 K	0.2162	10.062
100 K	0.3538	26.297

6.3.4. Dielectric studies

Figure 6.6 shows the plots of variations in dielectric constant (ε') and dielectric loss (tan δ) with temperature (300–500 K) for the BC-BT composite sintered at 870 °C for 4, 8, 12, and 16 h at 1 kHz. It is observed from Figure 6.6(a) that the dielectric constant at 1 kHz, increases with increase in temperature from 300 to 500 K. The value of ε' of the composite sintered at 4, 8, 12, and 16 h was found to be 6.3×10^2, 1.0×10^4, 2.0×10^4, and 5.3×10^3, respectively at 500 K. The values of ε' increase gradually due to the chemical micro-heterogeneities present in the composite. It is also observed that the value of ε' gradually increases with increasing sintering duration at a given temperature. The dielectric constant is almost temperature independent for the composite sintered for 4 h. The increase in ε' with increasing sintering duration may be attributed due to the growth of polarization with increasing sintering duration [Zheng *et al*. (2014)].

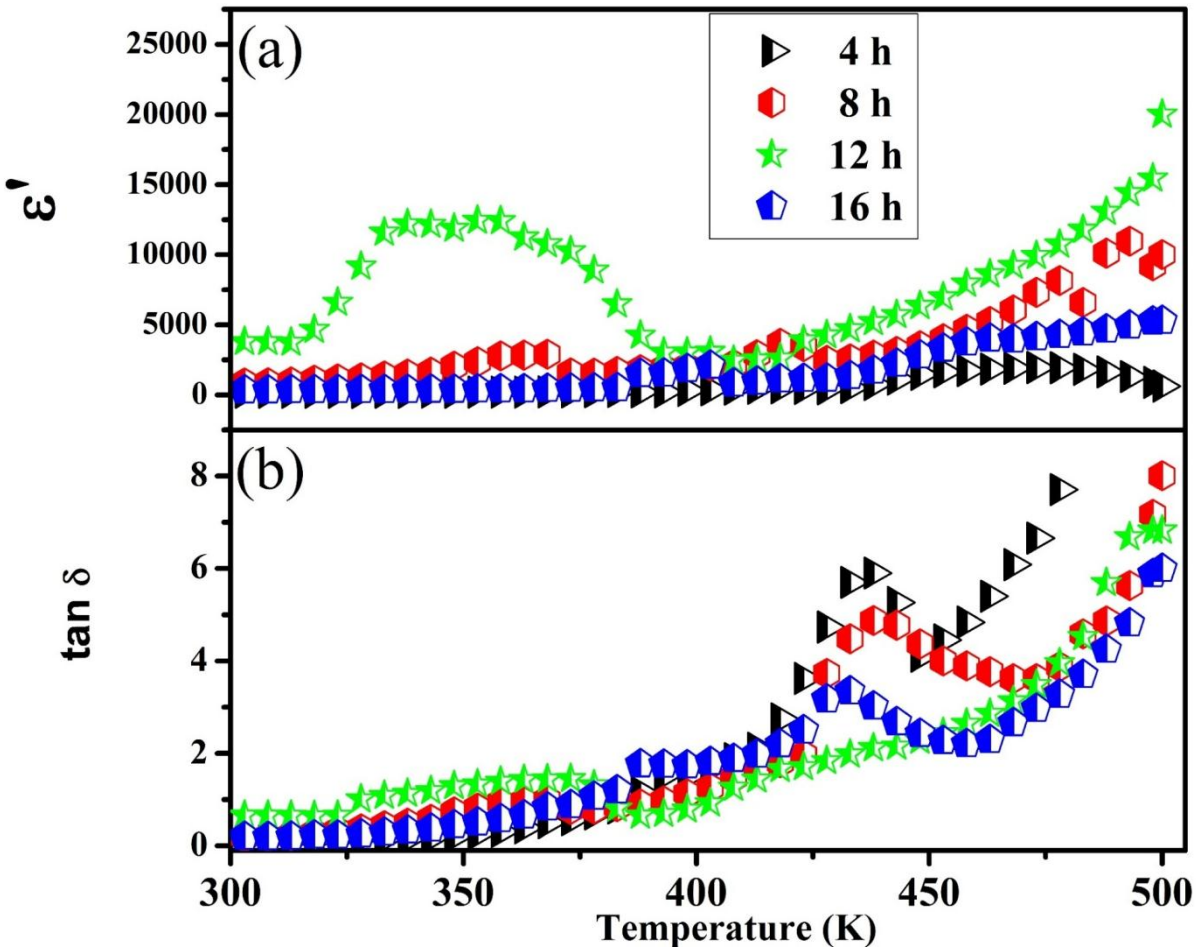

Figure 6.6. (a) Variation of the dielectric constant (ε') and **(b)** tan δ with temperature of BC-BT nanocomposite at 1 kHz for sintered at 870 °C for 4 h, 8 h, 12 h and 16 h.

Figure 6(b) clearly shows the temperature independent of tan δ from 300 to 400 K, and after that, it increases sharply. The relaxation peaks in the BC-BT composite are also observed. With increasing temperature, the amplitude of the relaxation peaks shifts to the lower sintering durations. The dielectric loss (tan δ) is strongly temperature dependent and increases sharply above 413 K. A ferroelectric relaxor is usually characterized by a diffuse phase transition and high relaxation dispersion in loss tangent (tan δ) indicates thermally activated relaxation [Chunhong *et al*. (2009)].

Figure 6.7(a) shows the plots of variations in dielectric constant (ε') as a function of frequency from 10^2 to10^6 Hz for the composite sintered at 870 °C for few selected durations (4, 8, 12, and 16 h). It is observed that the dielectric constant decreases rapidly below 100 Hz and then remains nearly constant between 10^4 and 10^6 Hz. The ε' value decreases with increasing frequency, while the dielectric constant increases at a given frequency with increasing sintering time.

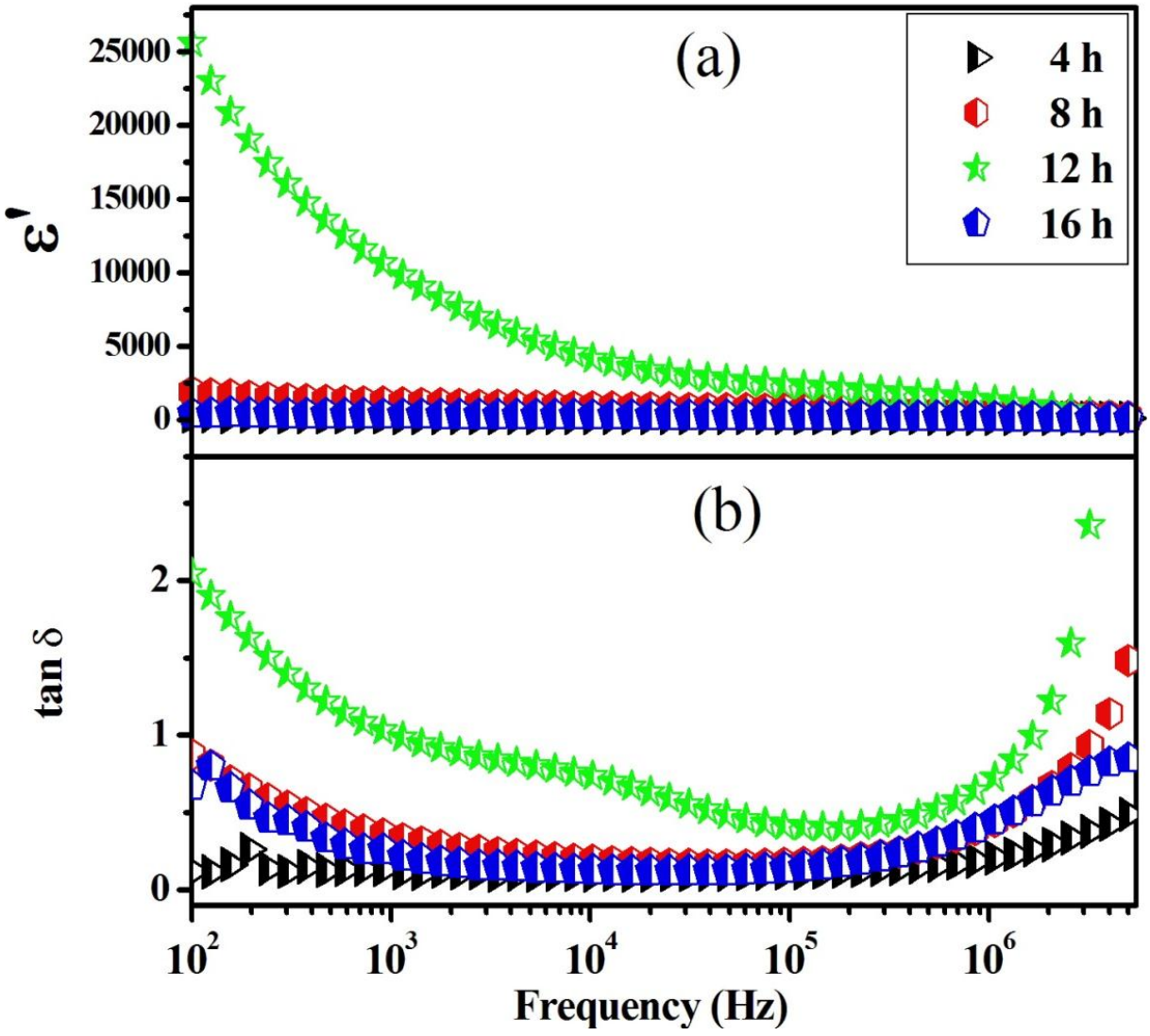

Figure 6.7. (a) Variation of the dielectric constant (ε') and **(b)** tan δ with frequency of BC-BT nanocomposite at 50 °C for sintered at 870 °C for 4 h, 8 h, 12 h and 16 h.

The dispersion in ε' with frequency can be attributed due to Maxwell–Wagner type of interfacial polarization, i.e. [Singh *et al*. (2014)] Hence, the interfacial polarization revealed a rapid rise in the dielectric constant for the composite sintered for a long duration at the frequency. Figure 6.7(b) shows the variation of loss tangent (tan δ) vs. frequency for the composite sintered at 870 °C a few selected durations. The frequency dependence of tan δ shown in the figure indicates that tan δ decreases rapidly over the entire frequency range. This may be due to the presence of small interfacial polarization in these materials [Mandal *et al*. (2009)]. At 4 h, tan δ is almost frequency independent up to 10^5 Hz. Especially, the dielectric loss of the BC-BT ceramic with 4 h sintering duration is lower than that of corresponding to other sintering durations.

6.3.5. Conductivity and impedance studies

Figure 6.8 shows the AC conductivity (σ_{ac}) as a function of frequency from 10^2 to10^6 Hz at 50 °C for the nanocomposite sintered at 870 °C for 4, 8, 12 h and 16 h. The conductivities show a dispersion pattern which shifts toward higher frequency with increasing sintering time. It is concluded that the conductivity increases with increasing sintering time. This recommended that at high frequencies, the AC conductivity is frequency independent but at lower frequencies, the AC conductivity increases, following Jonscher power law behavior [Jonscher et al. (1977)].

$$\sigma_{total} = \sigma_{ac} + \sigma_{dc} \qquad (6.2)$$

$$\sigma_{ac} = A\omega^s \qquad (6.3)$$

Where A is the temperature dependent constant determining the magnitude of dispersion at high temperature, σ_{dc} is the DC bulk conductivity, and s is the power law exponential term

known as exponent representing the degree of interaction between mobile ions which varies between 0 and 1. For, s > 0 the electrical conduction is frequency dependent, while the conduction for s = 0 is frequency independent. The value of s was found to be 0.51, 0.49, 0.40 and 0.46 for sintering duration 4 h, 8 h, 12 h and 16 h respectively. The frequency dependent conductivity is explained due to the hopping of charge carriers in finite clusters frequency.

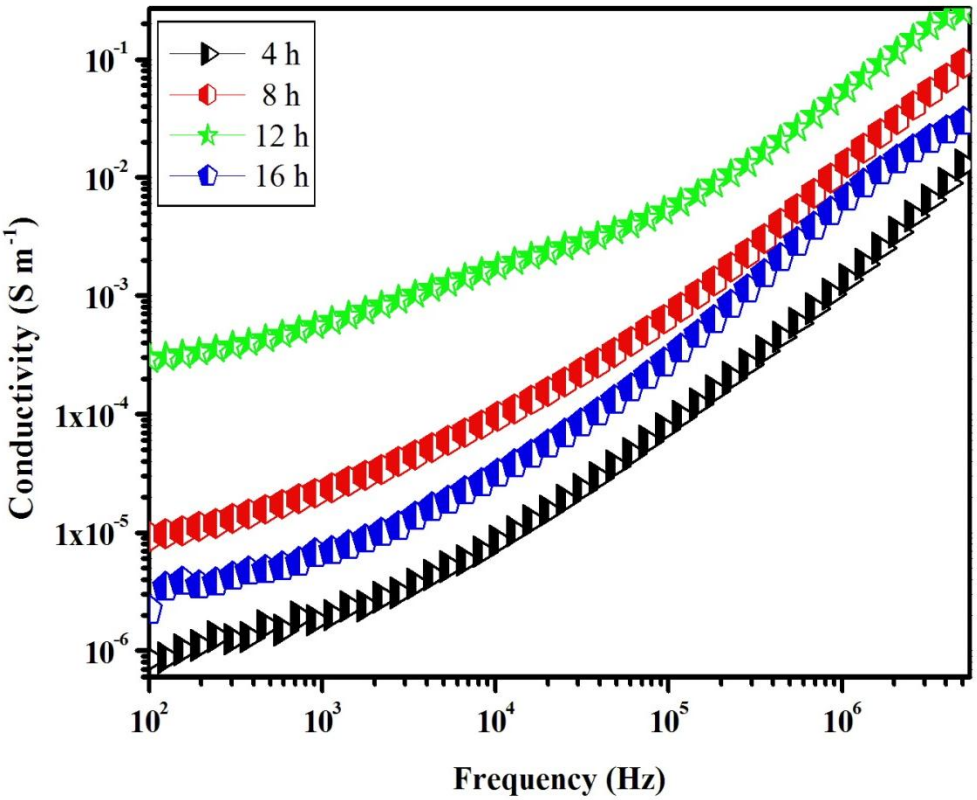

Figure 6.8. Plot of AC conductivity (σ_{AC}) vs. frequency at selected durations of BC-BT nanocomposite at 50 °C for sintered at 870 °C for 12 h.

Impedance analysis was conducted to separate the contributions of grains, grain boundaries, and an electrode to the total detected resistance in the nanocomposite ceramic. Typical complex impedance plots at 50 °C for the nanocomposite sintered at 870 °C for 4, 8, 12 h and 16 h are shown in Figure 6.9. Impedance spectrums are composed of two semi-circular arcs (a large one and a small one) with non-zero intercepts on Z' at the high-frequency end, which have different electrically active regions. They can be examined using a simplified equivalent circuit compose of two parallel resistance-capacitance elements [Mishra *et al*. (2008)].

The grains resistance (R_g) of BC-BT ceramic was found to be 150.80 Ω, 51.80 Ω, 37.30 Ω and 47.90 Ω sintered at 870 °C for 4 h, 8 h, 12 h, and 16 h, respectively. In the frequency spectrum, the position of the arcs depends on their sintering duration. Impedance plot gives two semicircles for grains (R_g) and grain boundaries (R_{gb}) at higher and lower frequency, respectively. The semicircles for (R_g) and (R_{gb}) become depressed with the decrease in the radius of the arc with increasing sintering duration which shows the increase in conductivity with increasing sintering duration for the BC-BT composite. Moreover, the radius of all the semicircles exhibits small shifts from the real axis, Z' which indicates that there is a distribution of continuous or discrete relaxation time around the mean relaxation time, $\omega_m\tau_m = 1$ [Rawat *et al*. (2012)].

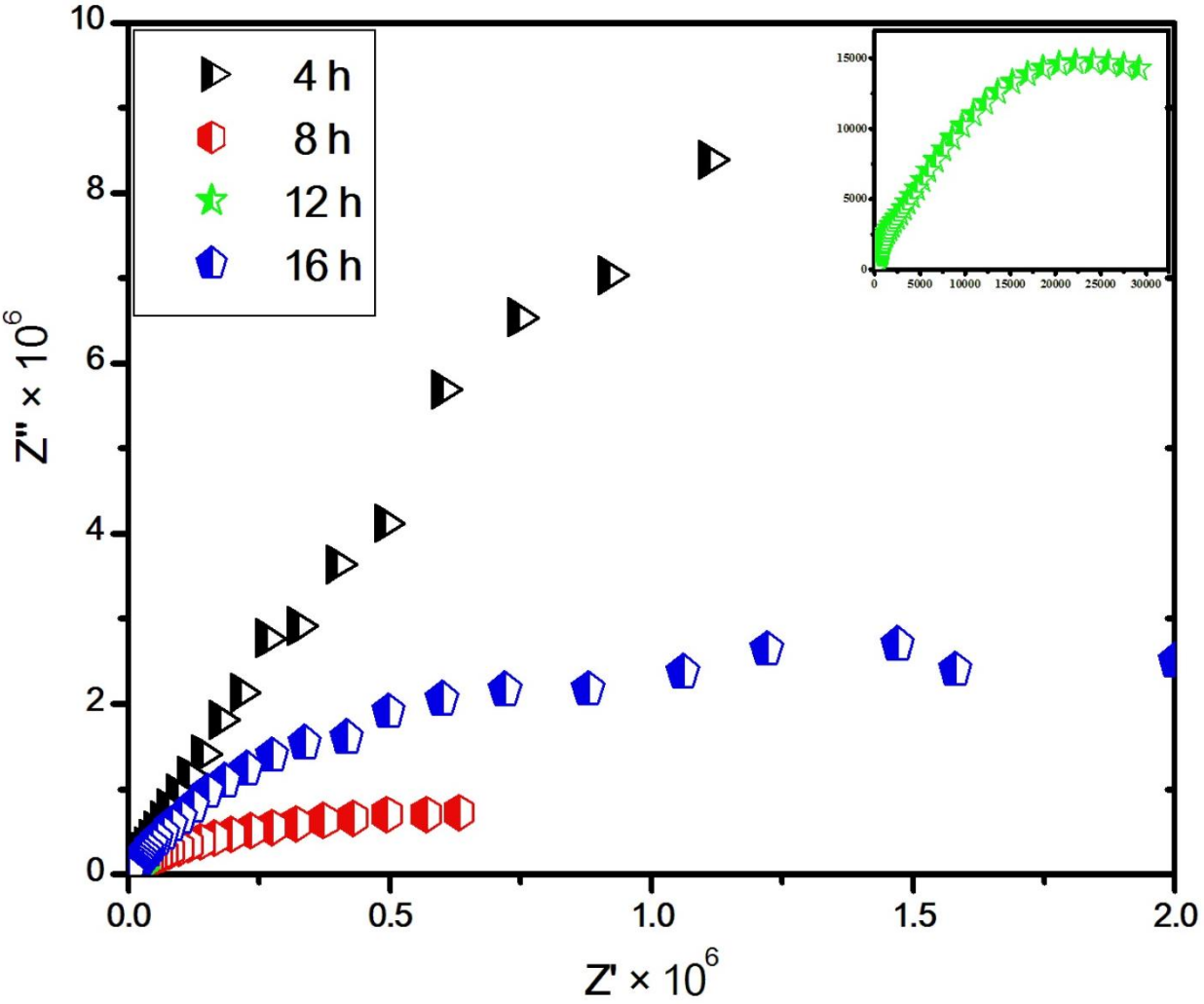

Figure 6.9. Impedance plane plots (Z' vs. Z'') and inset shows the expanded view of impedance plane plots (Z' vs. Z'') of the 12 h sintered close to the origin of BC-BT nanocomposite sintered sat 870 °C for 4 h, 8 h, 12 h and 16 h at 50 °C.

6.4. Conclusion

A nanocomposite $0.6Bi_{2/3}Cu_3Ti_4O_{12}$-$0.4BaTiO_3$ (BC-BT) with a particle size of 70±10 nm has been successfully synthesized by modified solid state route. X-Ray diffraction data confirm the presence of $BaTiO_3$ and $Bi_{2/3}Cu_3Ti_4O_{12}$ nanocrystalline phases co-existed in the nanocomposite. SEM and AFM studies suggest that grain boundary effects are responsible for enhanced dielectric permittivity and low value of tan δ in the BC-BT composite sintered

for short duration. The Magnetic behavior for the BC-BT composite ceramic revealed ferromagnetic with a weak magnetic moment and showed soft magnetically materials. The BC-BT ceramic shows temperature-independent dielectric performance at higher frequencies region. The exponent value (s) of the composite was found in the range of 0.40-0.51 for the BC-BT composite. Impedance studies confirmed that BC-BT ceramic is electrically heterogeneous with semiconducting grains and insulating grain boundaries. Hence, the interfacial polarization revealed a rapid rise in the dielectric constant at high temperatures and low frequency due to charge accumulate grain boundaries this is known as IBLC mechanism which is responsible for the high dielectric constant in the BC-BT composite ceramic.